INT. J. REMOTE SENSING, 2001, VOL. 22, NO. 6, 1779–1797

# Mapping successional boreal forests in interior central Alaska

S. L. USTIN and Q. F. XIAO

Department of Land, Air and Water Resources, University of California, Davis, CA 95616, USA; e-mail: slustin@ucdavis.edu

(*Received 28 September 1998; in final form 22 November 1999*)

**Abstract.** It is necessary to develop new satellite methods to monitor boreal forests responses to climate warming. Remotely sensed maps derived from hyperspectral Advanced Visible/Infrared Imaging Spectrometer (AVIRIS) data were developed and compared for the four conifer forest ecosystems at the Bonanza Creek Experimental Forest, a long-term ecological research site on the Tanana River flood plain near Fairbanks, Alaska. The site was first stratified into montane, lowland alluvial plain, and flood plain zones based on topography. A classification of six forest and three non-forest types was created from AVIRIS images and compared on a pixel-by-pixel basis to a published vegetation map, a classified SPOT (Satellite Pour l'Observation de la Terre) image, and a hybrid SPOT image and digital elevation model classification. A comparison of AVIRIS with SPOT results showed that the AVIRIS classification was consistently more accurate (74, 43, and 43% overall accuracy, respectively). Hyperspectral classification methods have promise for mapping forest ecosystems in other boreal regions when little or no ground data are available for validation. The time difference between the creation of these maps show that substantial ecosystem changes have occurred over the past 15 years, demonstrating the need for developing a capability to obtain cost-effective landscape characterization.

## 1. Introduction

Boreal ecosystems cover 1372 M ha hectares globally (Dixon *et al.* 1994) and little of it has been mapped using direct observational methods. Boreal forests (taiga) are an integral component of the global biosphere, containing about 25% of the stored terrestrial carbon, estimated to be 1150 Gt, with 84% stored in soil organic matter (Dixon *et al.* 1994). Changes in the amount or rates of carbon storage or emission in boreal forests could have significant effects on global biogeochemical cycles (Bonan 1991, Bonan *et al.* 1995, Malhi *et al.* 1999) and climate (D'Arrigo *et al.* 1987, Kemp, 1991, Bonan and Van Cleve 1992, Stocks *et al.* 1998). Most general circulation models (GCMs) predict that the boreal region is subject to significant warming over the next few decades due to increasing atmospheric concentrations of radiatively important trace gases (Houghton *et al.* 1990, Oechel 1995). Canada and Russia have recorded a 2–3°C temperature increase from winter and spring warming during the last 30 years (Stocks *et al.* 1998). Myneni *et al.* (1997) used the NOAA Advanced Very High Resolution Radiometer (AVHRR) record to show that extended phenological cycles and increased foliar biomass may have


ISSN 0143-1161 print/ISSN 1366-5901 online © 2001 Taylor & Francis Ltd
http://www.tandf.co.uk/journals

already occurred in north-western North America. In two decades of arctic measurements, Oechel *et al.* (1994, 1995) showed that $CO_2$ source and sink relations for $CO_2$ changed with interannual climate conditions.

Changes in the competitive relationships among successional forest could alter the distribution of late seral ecosystems (e.g. from conifer to broadleaf forest), changing total carbon storage and the proportion of above and below ground components (Bonan *et al.* 1990, Pastor and Mladenoff 1992, Lenihan 1993, Chapin *et al.* 1996, Oechel 1997). Other climate changes (e.g. the abundance and timing of precipitation) could extend summer drought and alter wildfire characteristics, the primary factor driving succession in boreal forests (Viereck 1983, Kasischke *et al.* 1995, French *et al.* 1997, Weber and Flannigan 1997, Weber and Stocks 1998). Changes in the spatial distribution or depth of permafrost, an interactive factor in the distribution of boreal forests, may also affect carbon storage or release (Halsey *et al.* 1995). Because of different energy and nutrient cycling characteristics among taiga ecosystems, such changes may further destabilize the ecology of the region through climate feedbacks (Bonan 1995). To understand the rate of change in boreal ecosystems, it is essential to have a baseline for monitoring forest distributions and characteristics over time.

The observations needed to monitor boreal ecosystem change (e.g. forest identification, successional stage, canopy closure, and stand density), at regional scales over periods of years to decades or longer, are difficult if not impossible with current mapping and inventory methods. Remotely sensed imagery offers the most practical opportunity to obtain accurate forest maps at local to regional scales, with a potential to update them at annual to decadal frequencies.

Current satellites have not succeeded in providing this assessment, because of infrequent overpasses during the growing season and poor spatial resolution, spectral resolution, data quality, or cost. However, several new satellite systems offer the potential to improve mapping: these include the imaging spectrometers, like NASA's New Millenium EO-1 satellite to be launched in 2000, U.S. Dept. of Defense's Warfighter and NEMO (Navy Earth Mapping Observer), and the Australian commercial sensor, AIRES, to be launched in 2001. The goal of this research was to use hyperspectral data to classify taiga vegetation types, using data from the NASA airborne high spatial and spectral imaging spectrometer (Advanced Visible/Infrared Imaging Spectrometer, AVIRIS). This sensor acquires 224 contiguous spectral bands (*ca* 10 nm band resolution) in the visible to short-wave infrared region for each 20 m pixel. We contrasted these results to those obtained from classifying a SPOT (Satellite Pour l'Observation de la Terre), three-band (visible to near-infrared) sensor but acquired at similar spatial resolution. We compared these results to a SPOT classification by Rignot *et al.* (1994) and a hybrid digital elevation model (DEM) and SPOT classification by Ustin *et al.* (1994). The high resolution of the SPOT and AVIRIS images allowed us to evaluate the spatial scales and the spectral resolutions needed to identify forest ecosystems in the boreal region.

### 1.1. *Boreal forest ecosystems*

The boreal forests of Alaska are floristically simple, with only nine tree species dominating the region (Takhtajan 1986). These ecosystems are composed of late seral forests, dominated by black spruce (*Picea mariana*) or white spruce (*P. glauca*) and several early and mid-succession deciduous broadleaf forests that include alder (*Alnus tenuifolia*), paper birch (*Betula papyrifera*), aspen (*Populus tremuloides*), and balsalm poplar (*P. balsamifera*). These species typically occupy different stages in ecological succession, with broadleaf species dominating earlier seral stages relative to conifers. The forests are structurally simple, a single-layer closed-canopy or an open-canopy stand with a moss and ericaceous shrub understory. The presence of a thick sphagnum moss layer in spruce forests is an important factor in the development of permafrost. Fire history is a major determinant of ecosystem structure, with frequent wildfires creating a complex spatial mosaic; it is also a major factor in determining the proportion of living and dead biomass found in these forests (Kasischke *et al.* 1995, Stocks *et al.* 1998, Weber and Stocks 1998).

The Bonanza Creek Experimental Forest (BCEF) in Alaska contains the four late seral boreal forests described by Van Cleve and Viereck (1981): (1) flood plain white spruce, (2) upland white spruce, (3) lowland black spruce, and (4) upland black spruce. Mid-successional broadleaf forests include alder and balsam poplar and conifer/hardwood mixtures. Upland white spruce succession includes aspen and paper birch phases, while black spruce includes only a paper birch phase. Flood plain white spruce starts with a shrub stage and invasion by willows, followed by alder and balsam poplar phases (absent from the lowland black spruce sequence). Flood plain white spruce undergoes a transition to lowland black spruce if succession continues undisturbed for an extended period.

Topography, especially elevation and aspect, is critical in determining the potential distribution of the dominant species in the upland forests. Soil factors, primarily drainage, temperature, and permafrost, are also significant in controlling species distributions (Bonan *et al.* 1992, Van Cleve *et al.* 1993). As forests undergo succession, changes in canopy cover and the depth of organic matter in the forest floor alter the energy budget and change a site from permafrost-free to permafrost-dominated (Viereck 1983, Oechel and Lawrence 1985).

## 2. Methodology

### 2.1. *Study area*

The study site at the BCEF long-term ecological research (LTER) area is located approximately 40 km south-west of Fairbanks, Alaska (64° 45′ N, 148° 15′ W). Rounded hills and ridges dissect most of the area north of the Tanana River (crossing east–west) with many drainage systems (figure 1). These hills are part of the unglaciated Yukon–Tanana uplands of Precambrian Birch Creek schist which are overlain by loessal deposits from the Tanana River (USDA SCS 1977, Viereck *et al.* 1993a). The geology around and south of the river contrasts sharply, as the flood plain was formed by Pleistocene glaciers that left broad outwash plains and gravel moraines. The climate is continental with pronounced temperature extremes and a rapid change from cold to warm seasons, with the region having 80 + frost-free days per year (USDA SCS 1977, Viereck *et al.* 1993b). The meandering Tanana River flood plain consists of erosional cut banks and deposition silt bars that create a mosaic of successional forests. Permafrost is discontinuous within these stands. In the lowlands, both white and black spruce occupy the same topographic zone, as do alder, balsam poplar, and paper birch.

### 2.2. *Datasets*

A DEM of the site was obtained from the U.S. Geological Survey at 2- × 3-arc-second spacing and resampled to 20 m × 20 m horizontal resolution and 9 m vertical resolution, covering the area from 7 168 020 N to 7 185 420 N and 435 720 W to

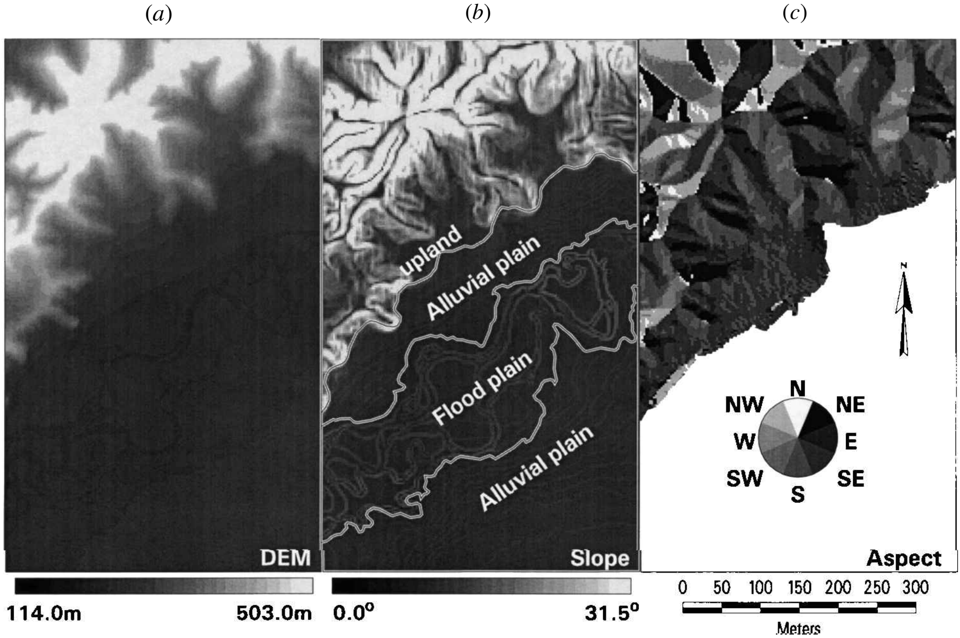


Figure 1. Digital terrain images for the BCEF: (*a*) gray-scale elevation image; (*b*) gray-scale slope classes; (*c*)gray-scale aspect map.

446 090 W (UTM, Zone 6). This corresponds to maps C-3 and D-3 Fairbanks, AK1:63 360 quadrangles. The study area reported covers the area between 427 947 W to 452 919 W and from 7 152 915 N to 7 209 164 N. Maximum site elevation is 503 m.

An unpublished digital vegetation map of the BCEF LTER site was assembled from interpretation of 1978 aerial photos and field surveys and provided by J. Yarie (Department of Forest Sciences, University of Alaska, Fairbanks). The map was assembled in 1992 in collaboration with E.F. Binnian (USGS, EROS Alaska Field Office, Anchorage). Rignot *et al.* (1994) established that the BCEF map does not reflect changes in the river course since 1978, vegetation changes resulting from the 1983 Rosie Creek fire (fire boundary provided by Alaska Fire Service, Fairbanks), and changes due to logging and stand development. Nonetheless, this is the most complete dataset available for validating remotely sensed maps of forest composition at the watershed scale. The smallest mapped parcel area was 1039 $m^2$. The 1993 digital version of this map is an ARC/Info (ESRI, Redlands, CA) coverage and was used to georeference the SPOT image by co-registering to 21 control points in ARC/Info. The AVIRIS image was registered to the SPOT image for the area coincident with BCEF coverage. Registration to precise geographic coordinates is difficult, especially in the aluvial plain and riparian zones, because there are no topographic or consistent geographic features in that region. The Tanana River channel changes frequently, so the image and map locations do not match. There are no roads or other features to precisely match locations that are south of the river.

The digital vegetation distribution map of the BCEF provided by the Forest Service included 100 map categories which were merged into seven forest classes following a simplified paper-copy scheme provided by the LTER, consistent with the principal interior boreal forest successional types. The consolidation step merged different stocking densities and crown closures into a single forest type and mixed forest classes with the dominant forest type. We did not analyse the effect of class consolidation, so some errors are attributable to heterogeneous stand variability. The BCEF map includes a heterogeneous 'non-forest' class composed of low ericaceous shrubs, mosses/muskeg, or lands of other undefined disturbance characteristics, e.g. roads and recently logged or burned sites.

An unpublished digital soils map of the uplands area was obtained from the United States Department of Agriculture (USDA) Natural Resource Conservation Service (NRCS) in Alaska and imported into Arc/Info using the published soil survey maps (USDA SCS, 1977) of the Goldstream–Nenana area, Alaska, to define the polygon attributes.

AVIRIS images (950614B0201) were acquired over the BCEF LTER site on 14 June 1995. Scenes two and three were merged and an area of 10 km × 17 km was analysed. Sky conditions were mostly clear at the time of acquisition, but clouds and cloud shadows were located near the lower right and centre of the scene, with several smaller clouds near the upper left side of the scene. Data were calibrated to apparent surface reflectance using the ATmosphere REMoval Program (ATREM 2.0, University of Colorado) based on a modified version of the Modtran III radiative transfer atmospheric code. Thirty-eight bands were eliminated (1–5, 107–116, 152–169, 220–224), those that either had near-zero reflectance, low radiometric variability and/or were noisy. A linear mixture analysis was performed in IDL/ENVI 3.0 (RSI, Boulder, CO) using image selected endmembers for clouds, bare soil, green vegetation, dry plant litter, and water/shade. The identity of the endmembers was confirmed using vegetation polygon boundary overlays. The first step was to identify cloud pixels using the endmembers. These pixels were masked, a subsequent unmixing on the remaining pixels was performed, and these data were used in vegetation analyses. A supervised maximum likelihood classification (MLC) was obtained using the endmember images.

A Satellite Pour l'Observation de la Terre (SPOT-2) multispectral (HRV-2 mode) image of the region was acquired under clear skies on 28 August 1991. The nominal pixel resolution of SPOT and AVIRIS is the same at 20 m. The Normalized Difference Vegetation Index (NDVI) was computed using red and near-infrared bands $(3-2)/(3+2)$. Supervised MLC procedures cited by Rignot *et al.* (1994) were followed to reproduce their results for comparison to AVIRIS results. Band 3 (near-infrared) was used to map the Rosie Creek fire boundary, a 6000 ha wildfire located north of the Tanana River.

### 2.3. *Classification procedure*

The initial step in our analysis was to divide the study area into upland and lowland regions based on topography (figure 1). The lowland boundary was defined as the upper edge of the Tanana River alluvial plain at the transition where the elevation contours become closely spaced (figure 1 (*a*)) and the slope angle increases rapidly (figure 1 (*b*)). The lowland region was separated into two regions, the flood plain region immediately around the Tanana River and the spatially intermediate alluvial plain. The aspect image is shown in figure 1 (*c*). The north-west corner of the image has extensive exposures on north and west facing slopes in contrast to the more central upland region, which has more south and east facing slopes.

### 2.4. *Spectral Mixing Analysis (SMA) methods*

SMA of hyperspectral data has advantages for land cover classification. It provides assessments of general landscape properties and does not require independent ground-based training sets to perform the image analysis. SMA reduces the dimensionality of the AVIRIS data but retains the spectral information. It characterizes the fractional contribution to the pixel reflectance using standard land cover categories, including the green foliage fraction, the litter/wood fraction, soil fraction, shadow/shade fraction, and cloud fraction (Smith *et al.* 1990, Roberts *et al.* 1993). The foliage, litter, and soil fractions have been shown to vary with the characteristics of different land cover types (e.g. Gamon *et al.* 1993, Roberts *et al.* 1993, Ustin *et al.* 1994, 1998) and can be secondarily used in maximum likelihood classifiers to characterize different vegetation types.

### 2.5. *Accuracy assessment*

Analysis was performed on the original predictions, with no smoothing or clustering of results and no masking for polygon boundaries to improve accuracy. Despite obvious errors in the map boundary locations, the decision to report all pixel results was made (1) because of the number and size of polygon parcels created a large number of 'edge' pixels, which would significantly impact the analysis and possibly introduce uncontrolled bias; and because (2) we had no other objective way to eliminate pixels; and (3) no objective way to subsample validation data for map comparisons. A significant literature has developed on classification accuracy assessments, and various methods have been proposed to improve map accuracy (e.g. Edwards *et al.* 1998, Richards 1996, Stehman 1996, Steele *et al.* 1998, Stehman and Czaplewski 1998). Most studies are faced with developing a validation set using a stratified point sampling design; however, field validation plots and a vegetation map were already available for this study. Selection of random pixels (whether edge masked or not) improves the classification accuracy statistics but does not affect the resulting map or its actual quality. Because we had no rationale for selecting or ignoring mapped pixels, we chose to accept poorer statistics with a full comparison of all pixels. Mis-registration of datasets is another common problem encountered, as is difference in time when maps are produced (Stehman and Czaplewski 1998). Co-registration of Geographical Information System (GIS) data layers was poor in the flood plain and riparian zones for these data, as described earlier. Therefore, despite clear evidence of mis-registration among datasets, we assumed that a minimum accuracy estimate was preferable. We chose to use the standard producers and users confusion matrix as the basis for comparison. The accuracy of the classification models was assessed on a pixel basis and an error matrix computed (Card 1982, Davis and Goetz 1990, Congalton 1991), which takes into account the omission and commission errors.

Rignot *et al.* (1994) reported an 83% overall classification accuracy using the same 1991 SPOT image segment for an area in the flood plain zone. To evaluate the accuracy of our mapping, we developed a supervised MLC using their training sites (Way *et al.* 1992), which we compared to the BCEF vegetation map. Training sites included 38 homogeneous ('pure type') forest stands of six forest types along the river, and a water class, which Rignot *et al.* (1994) included in their assessment. The analyses were performed for the riparian zone, lowland zone, and the full image area. The predictive maps from the MLC were then compared to the ground-based vegetation map from the BCEF for accuracy and to our classification analyses using AVIRIS.

## 3. Results

### 3.1. *Classification of boreal forest ecosystems*

#### 3.1.1. *Distribution by elevation and aspect*

The upland and lowland regions are clearly separable (figure 1); Bonanza Creek Watershed rises steeply in the north-east quadrant. However, the lowland alluvial plain and the flood plain forests were not readily separable due to the coarse elevation resolution. The boundaries seen in figure 1 (*b*) depict the position of the Tanana River flood plain at the time the topographic map was produced (based on 1952 and 19543 photos, produced in 1976) and the broader alluvial plain region, which includes older oxbow lakes and river terraces. The relationships between forest types and aspect (figure 2) shows the widespread distribution of white spruce on north-east to south-west aspects and more restricted black spruce on the north-west aspect. The abundance of aspen on the north-east to south-west aspects and balsalm poplar in the west and north-west aspects suggests why these forests are succeeded by both white and black spruce types. Paper birch is successional to both white and black spruce, and its distribution at the BCEF on all aspects supports this relationship.

#### 3.1.2. *Differentiation of boreal forests based on the BCEF vegetation map and topography*

The BCEF data show the study area to be divided nearly equally between lowland (54%) and upland (46%) forest ecosystems. The distribution of forests across elevational zones varies widely. In both upland and lowland forests, the black spruce successional sequence covers a greater total area then the white spruce seral sequences (table 1). The montane zone black spruce forests are six times the spatial extent of white spruce but about equally abundant in the lowland (flood plain and alluvial plain) area. In terms of the distribution of late seral stage forests, however, black spruce is only half as abundant as white spruce in the montane area but is 1.6 times more abundant in lowland forests. Only a small fraction of the land area is classified as non-forest (17% lowlands and 14% montane), also indicating that most of this landscape is at the relatively late seral stages (conifer or mixed conifer classes).

#### 3.1.3. *The 1983 Rosie Creek fire*

The Rosie Creek fire scar, extending over four subbasins along the upland reaches of the Tanana watershed is shown in figure 3 (*a*). The mapped location of the wildfire boundary shows significant disagreement, in some regions exceeding a kilometre offset with the registered 1991 SPOT image. This demonstrates the difficulty in accurately field-mapping vegetation boundaries and in precise co-registration. The fire occurred prior to the availability of accurate Global Positioning System (GPS) mapping methods, one reason for this disagreement. Some vegetation islands within the fire boundary were not burned, and these patches are outlined in the image. Re-vegetation, ground cover, and soil variability contribute to brightness variation within the fire scar in the near-infrared image.

#### 3.1.4. *1991 SPOT NDVI image*

Significant spatial patterns are observed in the NDVI image that correspond generally with the three terrain classes, but heterogeneity within the terrain regions resembles vegetation patterns (figure 3 (*b*)). Very low vegetation values occur in the fire scar, which is easily evident 8 years after the fire. Low NDVI values are also found across the alluvial plain zone, both north and south of the Tanana River, compared to significantly higher values in the flood plain and in the upland zones.

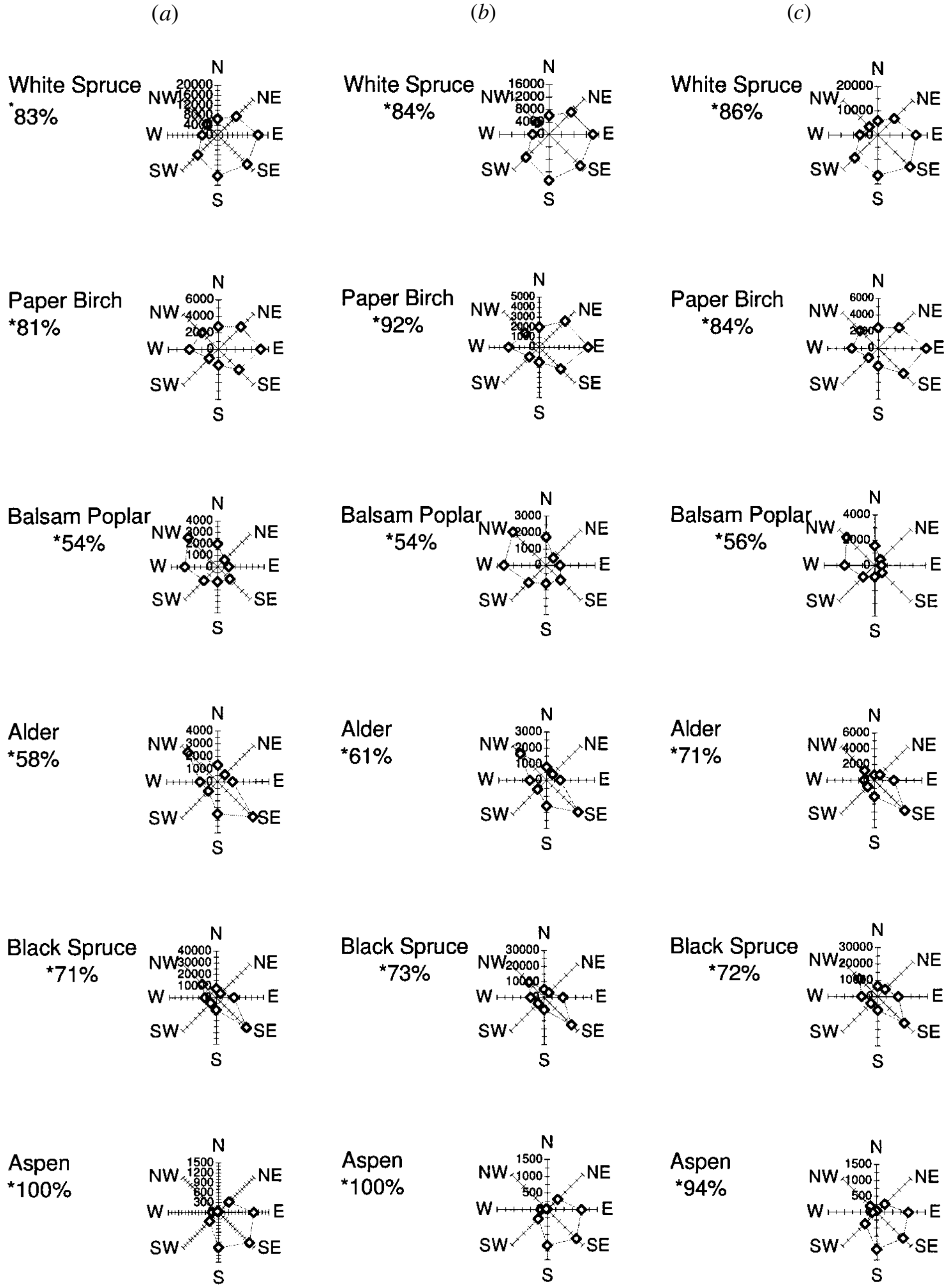


Figure 2. Aspect distribution of the dominant forest species at the BCEF; (*a*) from the BCEF base map; (*b*) from the BCEF base map eliminating areas under the AVIRIS cloud mask from the analysis; (*c*) predicted from AVIRIS classification. The percentage shown under the forest type names identifies the proportion of the area occupied by that type with a defined aspect (i.e. not level terrain). The numbers on the ordinate indicate the number of pixels having that aspect.

Table 1. Total areas of upland and lowland forests that represent different seral stages in the ecosystems of the BCEF (total study area 170 km$^2$).

| | Uplands (% area) | | Lowlands (% area) | |
|---|---|---|---|---|
| Forest type | BCEF map | AVIRIS prediction | BCEF map | AVIRIS prediction |
| White spruce sere | 53.4 (82314) | 59.6 (91871) | 40.9 (74062) | 31.3 (48248) |
| White spruce (climax) | 44.2 (68133) | 50.0 (77073) | 23.7 (42916) | 15.6 (24047) |
| Black spruce sere | 32.2 (496035) | 35.0 (53951) | 44.0 (79676) | 47.8 (86557) |
| Black spruce (climax) | 25.4 (39153) | 27.8 (42853) | 39.4 (71346) | 43.1 (78046) |
| Other classes (sere) | 14.4 (22197) | 5.4 (8324) | 15.1 (27343) | 20.1 (36397) |
| Total (%) | 100 | 100 | 100 | 100 |
| Region | No. cells correct | Total cells | | |
| Montane | 108261 | 133019 | | |
| Alluvial Plain | 58122 | 84187 | | |
| Flood Plain | 34661 | 56106 | | |

3.1.5. *The endmember images*

The green foliage vegetation endmember from the 1994 AVIRIS data (figure 4 (*a*)) shows some consistency in spatial patterns with the older NDVI image. The darkest patch, observed in the centre of the image, and a patch in the lower right, are from clouds and cloud shadows. In general, the fire scar appears to be reduced in size due to regrowth during the 4 years between acquisitions. While patterns are similar, the dynamic range is greater and the AVIRIS data appears to be more detailed, despite similar pixel resolutions.

The dry vegetation endmember (figure 4 (*b*)) is bright in areas with high concentrations of plant litter and wood. In this view of the data, the Rosie Creek fire scar stands out as having high amounts of litter and woody debris. However, other areas, particularly in the flood plain zone, stand out as having high litter concentrations. The spatial pattern observed in the distribution of litter abundance is not apparent in the NDVI image or in the green vegetation image.

Few pixels are dominated by bare soil (figure 4 (*c*)). Bare soil/gravel (bright values) is abundant on the unpaved road, creeks, gravel bars, and in the Tanana River. The latter is due to both the shallowness of the river and the rock powder and sediment in the meltwater. The cloud and cloud shadow cause some confusion in the SMA results, having values of intermediate soil fractions. Low values occur in the flood plain (where dry plant litter is high) and in parts of the uplands where green foliage cover is high.

The shadow endmember, a measure of illumination of the pixels (figure 4 (*d*)) was used to map the cloud shadows within the scene. In this representation, higher values indicate the surface is darker and lower values indicate it is brighter. Areas that are shaded by topography have high shadow values. The shadow endmember image shows that high shadow values occur in the river and in other water bodies (such as the oxbow north of the river near the centre of the image), indicating that most incident photons are absorbed. Clouds and cloud shadows show strong contrast with the surface variation.

3.1.6. *Training set*

The forest polygons identified by Rignot *et al.* (1994) along the Tanana River flood plain are shown superimposed over the AVIRIS green vegetation image in


Figure 3. SPOT-2 HRV-2 image of the study area. (*a*) Band 3 (near-infrared) gray-scale image showing the 1983 Rosie Creek fire boundary (white line) and the Alaska Fire Service defined fire boundary (black line). Mis-registration between the image and the database map is evident. The road and Tanana River are near white areas, and logging (e.g. near road) has sharp geometric boundaries surrounding bright zones. (*b*) NDVI image shown as a gray-scale image. Lowest vegetation values are black (i.e. no vegetation) and highest vegetation values are white, over a linear gray-scale.

figure 5. Within the cloud mask and in surrounding areas, the BCEF vegetation map boundaries are shown. While the detailed patterns between the mapped boundaries and the green vegetation fractions show considerable correspondence, there are some obvious differences. The changes in the location of the Tanana River during the time between creation of the vegetation map and the image makes precise registration impossible. Clearly, mis-registration is evident as some patterns are similar but appear offset, often up to 0.5 km (25 pixels). It is also clear that the 'pure' forest classes are not always in agreement with the BCEF map boundaries, nor do polygons entirely coincide. Both the field polygons of homogeneous forest types and the BCEF polygons include unaccounted-for and significant heterogeneity in foliage fractions as observed in NDVI (figure 3 (*b*)) and green vegetation fraction (figure 4 (*a*)). Other errors may be attributed to either location errors in the original BCEF map or to changes in forest boundaries that have resulted from growth or logging between the times when the maps were produced.

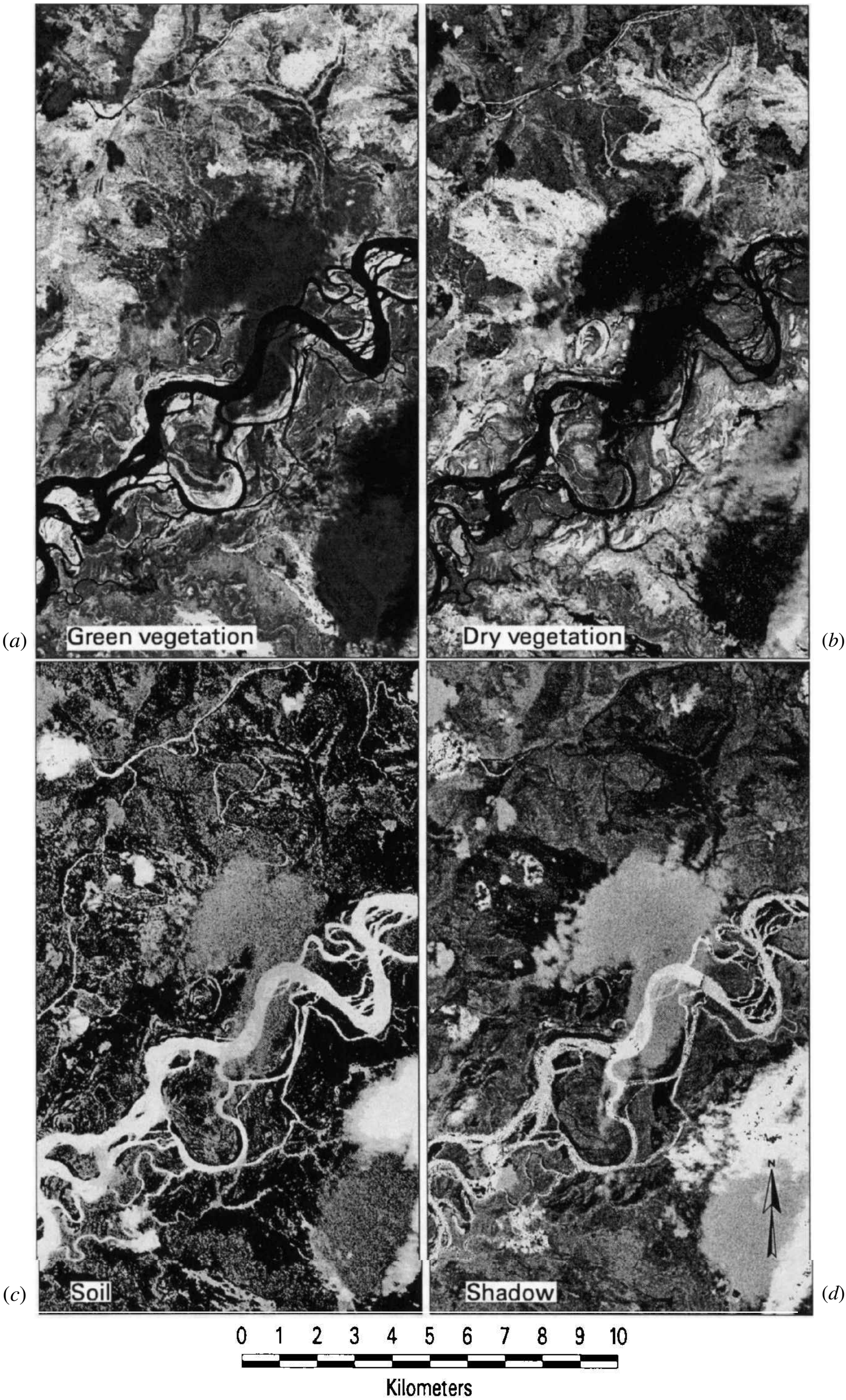


Figure 4. Fractional endmember maps for (*a*) green vegetation, (*b*) dry vegetation, (*c*) soil, and (*d*) shadow displayed as a gray-scale image. White indicates high pixel values and black low values (0–100%).

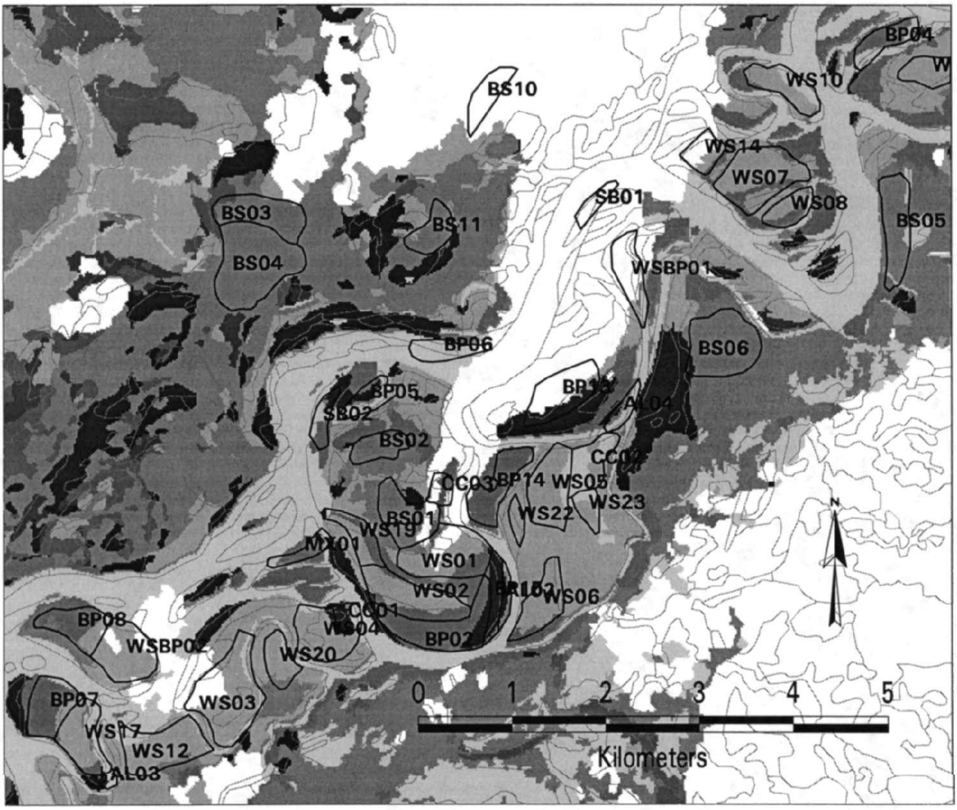


Figure 5. Training sites for 38 homogeneous forest stands in the flood plain of the Tanana River (ID numbers are shown). Training sites (dark line) superimposed on the AVIRIS gray-scale green vegetation endmember image. The clouds are masked and vegetation boundary contours from the BCEF map are shown in surrounding areas and under the cloud mask.

3.1.7. *Vegetation classification*

The false colour image of the vegetation endmember (red), dry vegetation (green) and soil (blue) is shown in figure 6 (*a*). Many of the vegetation patterns that are mapped in the ground-based map (figure 6 (*b*)) are readily observed without further classification. The most striking difference is the greater richness of pattern within the AVIRIS false colour fraction images than is found in the BCEF map.

The colour coded nine-class BCEF vegetation map is shown in figure 6 (*b*). The mixed forest classes were included within the dominant forest type; therefore, some classes are heterogeneous due to species mixtures and variability in stocking density. Crown closure is an additional source of variation and non-homogeneity.

The classification derived from the SPOT NDVI is shown in figure 6 (*c*). Almost the entire alluvial zone was mapped as black spruce, despite the presence of some patterns in the NDVI image. The montane and flood plain zones have patterns more consistent with the BCEF vegetation types, although paper birch was overestimated.

The classified AVIRIS forest map based on the fraction images is shown in figure 6 (*d*). The classes are neither smoothed or filtered to improve the fit. The

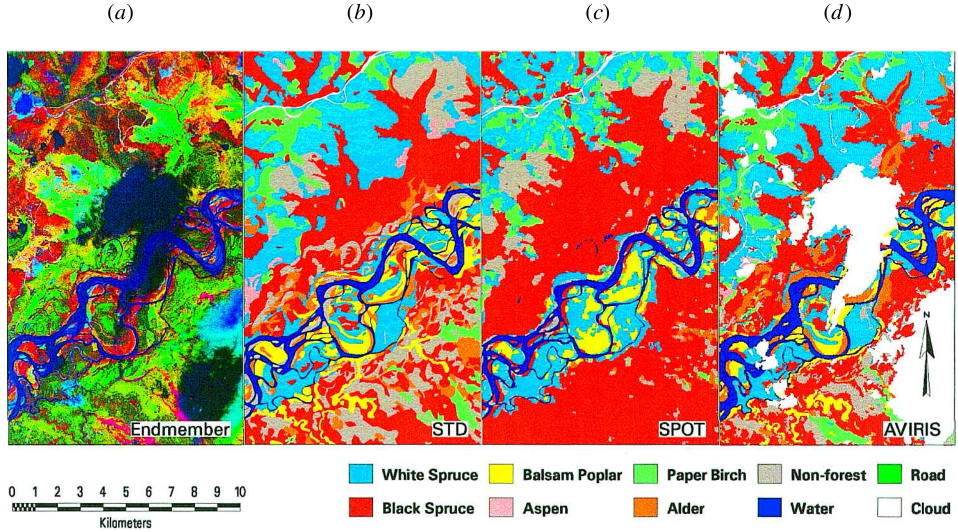


Figure 6. BCEF LTER vegetation maps: (*a*) false colour endmember image showing soil (blue), dry vegetation (red), and green vegetation (green); (*b*) BCEF basemap vegetation class; (*c*) classified SPOT image; (*d*) classified AVIRIS image (clouds and cloud shadow are masked). The forest type legend only applies to the classified vegetation maps.

distribution and size of the forest classes show considerable correspondence with the BCEF map. The clouds and cloud shadows are masked.

3.2. *Classification accuracy dependence on resolution of community type*

The accuracy assessment compares the proportion of ground-based vegetation types with predicted vegetation types on a pixel-by-pixel basis. Results are presented as the percentage correct in an error matrix (table 2). In our analysis, it was assumed that the ground-based map was accurate for the purposes of this study, since we had no field-validation points with which to assess its accuracy. The map had received preliminary evaluation by the Forest Service but had not been rigorously evaluated (L. A. Viereck, personal communication, 1994). Based on field evaluation of 38 pure stands in the riparian zone, Rignot *et al.* (1994) estimated that the BCEF map was 80% accurate, a value consistent with other field mapped parcels (Stehman 1996). Based on this criteria, we would not anticipate accuracy statistics to exceed the base map accuracy.

Overall, we found reasonably good agreement on an absolute pixel basis between the two maps, with much of the disagreement due to the differences in spatial scale between ground-based polygons and the raster images (table 2). If the more heterogeneous non-forest vegetation class is omitted, the overall pixel accuracy for agreement between the base map and the classified AVIRIS map is 74%. Classification accuracy varied with topographic zone, as shown in table 2. In general, the accuracy is highest for the most common forest types. Accuracy ranged from 50 to 78% in the flood plain zone, from 30 to 67% in the alluvial plain zone, and from 63 to 83% in the montane zone.

To evaluate the AVIRIS map, a supervised MLC was done using the training set described by Rignot *et al.* (1994) on the three SPOT bands. Most commission errors arose by mis-classification into a related forest type, e.g. white spruce rather than

Table 2. Supervised classification error matrix (percentage of pixels matched) for six classes of forests, showing errors in the three topographic zones for the site. The rows show the distribution of the class in AVIRIS pixels, and the columns show the distribution of the AVIRIS class in the BCEF base map. The overall accuracy for all classes is 65%, and the overall accuracy for forest classes (excluding 'non-forest' class) is 74%. If a type is absent from the zone, it is omitted from the table.

| Base map | Roads | Non-forest | White spruce | Paper birch | Alder | Black spruce | Aspen | AVIRIS total |
|---|---|---|---|---|---|---|---|---|
| A. Montane zone | | | | | | | | |
| Roads | 73 | 2 | 3 | 2 | 0 | 1 | 0 | 81 |
| Non-forest | 2 | 0 | 0 | 0 | 0 | 0 | 0 | 2 |
| White spruce | 7 | 80 | 81 | 8 | 12 | 6 | 17 | 211 |
| Paper birch | 8 | 2 | 4 | 83 | 1 | 3 | 8 | 109 |
| Alder | 3 | 1 | 2 | 0 | 83 | 7 | 2 | 98 |
| Black spruce | 8 | 14 | 8 | 5 | 0 | 83 | 10 | 128 |
| Aspen | 0 | 0 | 1 | 0 | 4 | 0 | 63 | 68 |
| Base total | 100 | 100 | 100 | 100 | 100 | 100 | 100 | |

| B. Alluvial plain zone | Non-forest | Water | White spruce | Paper birch | Balsam poplar | Alder | Black spruce | Aspen | AVIRIS total |
|---|---|---|---|---|---|---|---|---|---|
| Non-forest | 37 | 0 | 1 | 3 | 3 | 19 | 6 | 0 | 69 |
| Water | 0 | 45 | 4 | 0 | 1 | 0 | 0 | 0 | 50 |
| White spruce | 3 | 1 | 36 | 0 | 1 | 3 | 4 | 0 | 48 |
| Paper birch | 14 | 0 | 8 | 67 | 0 | 10 | 3 | 40 | 142 |
| Balsam poplar | 3 | 26 | 1 | 8 | 55 | 1 | 3 | 0 | 97 |
| Alder | 7 | 0 | 3 | 0 | 0 | 30 | 6 | 4 | 50 |
| Black spruce | 36 | 28 | 40 | 22 | 40 | 36 | 77 | 9 | 288 |
| Aspen | 1 | 0 | 6 | 0 | 0 | 1 | 1 | 48 | 57 |
| Base total | 100 | 100 | 100 | 100 | 100 | 100 | 100 | 100 | |

| C. Flood plain zone | Non-forest | Water | White spruce | Balsam poplar | Alder | Black spruce | AVIRIS total |
|---|---|---|---|---|---|---|---|
| Non-forest | 5 | 0 | 3 | 1 | 0 | 1 | 10 |
| Water | 50 | 80 | 7 | 11 | 21 | 7 | 176 |
| White spruce | 6 | 8 | 69 | 17 | 8 | 6 | 114 |
| Balsam poplar | 12 | 6 | 8 | 51 | 7 | 3 | 87 |
| Alder | 10 | 3 | 7 | 9 | 50 | 4 | 83 |
| Black spruce | 16 | 3 | 7 | 11 | 13 | 78 | 128 |
| Base total | 100 | 100 | 100 | 100 | 100 | 100 | |

black spruce. We obtained an 86% pixel accuracy, compared to 83% reported by Rignot *et al.* (1994), using their training sites along the Tanana River and a mask limited to the same area. Their MLC was shown to be highly accurate when the analysis was confined to the flood plain zone from which the training sites were derived. It had higher accuracy then our AVIRIS classification for this area (83% versus 67%), since our results were based on an analysis of the entire site and not tuned to this zone. However, once their MLC was expanded to include the alluvial plain using the same vegetation categories, their classification accuracy decreased to 30%, while ours was still 69%. The reduction in accuracy is a primarily a consequence of the classifier dependence on the adequacy of the training set when it is applied beyond the range of variability over which it was developed. The decline in accuracy of the MLC in this zone is also due to the spatial mis-registration of vegetation patterns south of the Tanana River, the changes in vegetation within the Rosie Creek fire scar (which was partially regrown by 1995), and the spectral class identification. The significant loss of accuracy in the Rignot *et al.* (1994) result when expanded from the flood plain zone to the alluvial plain zone was unexpected, as the same forest types occur and topography does not affect radiance values. When the MLC analysis is extended to the full image area, the SPOT accuracy declines to 43%, in contrast to the overall AVIRIS accuracy of 74%. The alluvial plain zone had the lowest map accuracy in all methods.

Ustin *et al.* (1994) developed a rule-based classification for this site using a combination of elevation, slope, aspect, and NDVI to classify the same SPOT image for this scene. Nonetheless, their overall accuracy was only 43% for a seven-class map. Therefore, despite similarity in spatial patterns in the classified SPOT image and the BCEF map, more accurate mapping tools are still needed. Based on these results, imaging spectrometry data appears to have considerable potential to improve forest maps in the boreal region.

The overall map accuracy of 74% is in the same range as other reported forest accuracies (e.g. Congalton and Green 1993, Bigging *et al.* 1991, from photointerpretation; Gong *et al.* 1997, from AVIRIS using linear discriminant anlaysis; and Edwards *et al.* 1998, from Thematic Mapper (TM) derived Gap Analysis). Errors are also evident in the 'ground-truth' vegetation map. This is partly attributed to changes since the original photography was acquired in 1978. Further, some level of subjective decisions occurs in defining and locating the boundaries and in identification of forest and mixed forest communities in the BCEF map. Therefore, the true AVIRIS accuracy may be better then the minimum estimate obtained from this analysis, but which is well within confidence for existing boreal forest mapping. It is evident that the ground-based map is composed of fewer but larger polygons relative to the image-based predictions. Moody and Woodcock (1994) have shown that scale-dependent errors are a function of the original spatial resolution of the map and the fine-scale patterns of the class. Clearly, figure 5 shows heterogeneity within the training polygons, and boundary location errors are evident in figures 3 (*a*) and 5. Because forest succession cycles average 50–100 years (Viereck 1983), the most recent analysis, based on the 1978 photography, would identify a forest type that is actually 20–25% further into a seral fire cycle then indicated on the ground-based map. The Rosie Creek fire occurred within the mapped region in 1983 and remains clearly evident in the SPOT data, but it is not readily observed in AVIRIS data 5 years later. This fire (figure 3 (*a*)) primarily burned the mid-elevation white spruce forest.

### 3.3. *Relationships between vegetation and soil maps*

The NRCS soil survey maps of the Goldstream–Nenana area (1:31 680) were only available for the area north of the Tanana River. Comparisons between the soil units and the vegetation maps indicated some correspondence in patterns. This was particularly evident for the black spruce association on the Minto silt loam, Goldstream silt loam, and Tanana silt loam units. These soil series are associated with poorly drained soils and permafrost (USDA SCS 1977). Although vegetation type is used in delineating soil units, the relationship between specific vegetation types and soil units is complex, and including soil with the DEM in the SPOT classifier did not increase the accuracy of the vegetation map (Ustin *et al.* 1994). A histogram of each species (using the BCEF base map) was examined for forest associations with soil units. The deep well-drained loessial soils (e.g. the Fairbanks series or the Donnelly series) are not consistently associated with specific forests. White spruce was correlated with Fairbanks silt loam (60%), Balsam poplar with Fairbanks silt loam and Salchaket silt loam (71 and 97%, respectively), and aspen with Fairbanks silt loam (66%).

## 4. Discussion

Our analysis showed good prediction of the four major upland and lowland late seral forest ecosystems based on comparison to the BCEF vegetation map using a MLC derived from SMA using AVIRIS endmember images. The forest distribution map was in good agreement with the ground-based map, in terms of location and areal extent of forest distributions. The SPOT NDVI classified map was about half as accurate as the AVIRIS derived map, and the addition of soils and DEM data to the SPOT NDVI classifier did not approach the classification accuracy derived from SMA of AVIRIS data. Because the two sensors have similar 20 m pixel resolutions, the difference is attributable to the spectral coverage of AVIRIS images and retention of the spectral information in the SMA endmember maps. Clearly, the hyperspectral pixels were better able to identify vegetation types and were able to map vegetation variability within the BCEF polygons. The endmember classification model did not require field measured input, as they were derived from the images. One goal of this work was to use a simple methodology for analysing AVIRIS imagery, and one that did not require significant ground data to train the MLC.

The distribution of forest types with aspect, based on the AVIRIS classification (figure 2 (*c*)) closely follows the aspect distribution patterns for the forest classes in the BCEF map and is consistent in predictions of abundance (compare figure 2 (*b*) and (*c*)). Table 1 shows that the relative areal proportions of the landscape in white spruce and black spruce successional forests are consistent with the BCEF map in both lowland and upland habitats, but it indicates greater coverage of white spruce in uplands areas and less in lowlands areas (from 6.2 to −9.6%).

Production of the AVIRIS forest map provides information about the distribution of the four seral sequences and the fraction of the landscape in each type (table 2). The site is roughly equal between lowland and upland forest ecosystems, but the distribution of forest types varies significantly. If we assume the broadleaf seral forest sequences described in the introduction, and allow half the paper birch pixels to be assigned to each upland spruce type, we can estimate the distribution of these seral communities. Choosing an equal distribution of paper birch is a reasonable assumption, given its aspect distribution (figure 2). In the lowland forests, the black spruce successional sequence exhibits greater total area than white spruce seral sequences, while the reverse is true in the uplands area. The lowland black spruce forests are 1.5 times the spatial abundance of lowland white spruce. Table 2 shows that 90% of the lowland black spruce forest is at a late seral stage, while half of the flood plain white spruce is at a late seral stage. This partially reflects the loss of white spruce forests from the Rosie Creek fire. For the upland forests, about equal proportions of black spruce and white spruce forests are at a late successional stage (79 and 84%, respectively). The most interesting observation is the striking difference in the percentage of the forest in late seral stage between upland and lowland forests, which have opposite patterns for white and black spruce. Only a small fraction of the area is classified as non-forest (5.4%), also indicating that most of this landscape is at the relatively late seral stages (conifer or mixed conifer classes). Depending on the number of years a forest will remain in this initial phase of secondary succession, the actual turnover rates for these forests probably exceeds 100 years. Possibly, the differences in proportion of late seral stages in upland and lowland forests indicate a difference in the types of fires and the extent of combustion in these forests.

**Acknowledgments**

This research was performed under NASA EOS grant NAS-31359 and NAGW-2636 to the University of California, Davis. The analyses were performed on DEC Alpha computers provided under a Sequoia 2000 grant (Cooperative Research Agreement #1243) and a NASA Center of Excellence Grant (NRA-97-05). We wish to acknowledge that the ground-based vegetation maps and SPOT image used in this study were contributed by Dr JoBea Way (Radar Sciences Group, Jet Propulsion Laboratory, Pasadena, CA), Dr Les Viereck (Institute of Northern Forestry, Fairbanks, AK) and Dr. J. Yarie (University of Alaska, Fairbanks). The Alaska NRCS is gratefully acknowledged for providing their provisional soils map, and the Alaska Fire Service for the Rosie Creek fire map, and the USGS for the DEM.

**References**

Bigging, G. S., Congalton, R. G., and Murphy, E. ., 1991, A comparison of photointerpretation and ground measurement of forest structure. *ASPRS Technical Papers*, **3**, 148–157.

Bonan, G. B., 1991, Atmosphere–biosphere exchange of carbon dioxide in boreal forest. *Journal of Geophysical Research*, **96**, 7301–7312.

Bonan, G. B., 1995, Land–atmosphere interactions for climate system models: coupling biophysical, biogeochemical, and ecosystem dynamical processes. *Remote Sensing of Environment*, **5**, 57–73.

Bonan, G. B., Chapin, F. S., and Thompson, S. L., 1995, Boreal forest and tundra ecosystems as components of the climate system. *Climatic Change*, **29**, 145–167.

Bonan, G. B., Pollard, D., and Thompson, S. L., 1992, Effects of boreal forest vegetation on global climate. *Nature*, **359**, 716–718.

Bonan, G. B., Shugart, H. H., and Urban, D. L., 1990, The sensitivity of some high-latitude boreal forests to climatic parameters. *Climatic Change*, **1**, 2–29.

Bonan,G. B., and Van Cleve, K., 1992, Soil temperature, nitrogen mineralization, and carbon source–sink relationships in boreal forests. *Canadian Journal of Forest Research*, **22**, 629–639.

Card, D. H., 1982, Using known map category marginal frequencies to improve estimates of thematic map accuracy. *Photogrammetric Engineering and Remote Sensing*, **48**, 431–439.

Chapin, F. S., III, Hobbie, S. E., and Shaver, G. R., 1997, Impacts of global change on composition of artic communities: implications for ecosystem functioning, *Ecol. Studies*, **124**, 221–228.

Congalton, R., 1991, Review of assessing the accuracy of classifications of remotely sensed data. *Remote Sensing of Environment*, **37**, 35–46.

Congalton, R. G., and Green, K., 1993, A practical look at the sources of confusion in error matrix generation. *Photogrammetric Engineering and Remote Sensing*, **59**, 641–644.

D'Arrigo, R., Jacoby, G. C., and Fung, I. Y., 1987, Boreal forests and atmosphere–biosphere exchange of carbon dioxide. *Nature*, **329**, 321–323.

Davis, F. W., and Goetz, S., 1990, Modeling vegetation pattern using digital terrain data. *Landscape Ecology*, **4**, 69–80.

Dixon, R. K., Brown, S., Houghton, R. A., Solomon, A. M., Trexler, M. C., and Wisniewski, J., 1994, Carbon pools and flux of global forest ecosystems. *Science*, **263**, 185–190.

Edwards, T. C., Moisen, G. G., and Cutler, D. R., 1998, Assessing map accuracy in a remotely sensed, ecoregion-scale cover map. *Remote Sensing of Environment*, **63**, 73–83.

French, N. F. H., Kasischke, E. S., Johnson, R. D., Bourgeau-Chavez, L. L., Frick, A. L., and Ustin, S. L., 1996, Using multi-sensor satellite data to monitor carbon flux in Alaskan boreal forests. In *Biomass Burning and Climate Change*, edited by J. L. Levine (Cambridge, MA: MIT Press), pp. 808–826.

Gamon, J. A., Field, C. B., Roberts, D. A., Ustin, S. L., and Riccardo, V., 1993, Functional patterns in an annual grassland during an AVIRIS overflight. *Remote Sensing of Environment*, **44**, 239–253.

Gong, P., Pu, R., and Yu, B., 1997, Conifer species recognition: an exploratory analysis of *in situ* hyperspectral data. *Remote Sensing of Environment*, **62**, 189–200.

Halsey, L. A., Vitt, D. H., and Zoltai, S. C., 1995, Disequilibrium response of permafrost in boreal continental western Canada to climate change. *Climatic Change*, **30**, 57–73.

Houghton, J. T., Jenkins, G. J., and Ephraums, J. J., 1990, *Climate Change—The IPCC Scientific Assessment* (Cambridge, UK: Cambridge University Press).

Kasischke, E. S., Christensen, N. L., Jr, and Stocks, B. J., 1995, Fire, global warming and the carbon balance of boreal forests. *Ecological Applications*, **5**, 437–451.

Kemp, D., 1991, The greenhouse effect and global warming: a Canadian perspective. *Geography*, **14**, 121–130.

Lenihan, J. M., 1993, Ecological response surfaces for North American boreal tree species and their use in forest classification. *Journal of Vegetation Science*, **4**, 667–680.

Malhi, Y., Baldocchi, D. D., and Jarvis, P. G., 1999, The carbon balance of tropical, temperate and boreal forests. *Plant Cell and Environment*, **22**, 715–740.

Moody, A., and Woodcock, C. E., 1994, Scale-dependent errors in the estimation of land-cover proportions: implications for global land-cover datasets. *Photogrammetric Engineering and Remote Sensing*, **60**, 585–594.

Myneni, R. B., Keeling, C. D., Tucker, C. J., Asrar, G. and Nemani, R. R., 1997, Increased plant growth in the northern high latitudes from 1981 to 1991. *Nature*, **386**, 698–702.

Oechel, W. C., 1995, *Global Change and Arctic Terrestrial Ecosystems*, vol. 124, *Ecological Studies* (New York: Springer).

Oechel, W. C., Cowles, S., Grulke, N., Hastings, S. J., Lawrence, B., Roudhome, T., Riechers, G., Strain, B., Tissue, D., and Vourlitis, G., 1994, Transient nature of $CO_2$ fertilization in arctic tundra. *Nature*, **371**, 500–503.

Oechel, W. C., and Lawrence, W. T., 1985, Taiga. In *Physiological Ecology of Northern American Plant Communities*, edited by B. F. Chabot and H. A. Mooney (New York: Chapman and Hall), pp. 66–94.

Oechel, W. C., Vourlitis, G. L., Hastings, S. J., and Bochkarev, S. A., 1995, Change in arctic $CO_2$ flux over two decades—effects of climate change at Barrow, Alaska. *Ecological Applications*, **5**, 846–855.

Pastor, J. and Mladenoff, D. J., 1992, Southern boreal – northern hardwood forest border. In *A Systems Analysis of the Global Boreal Forest*, edited by H. H. Shugart, R. L. Leemans and G. B. and Bonan (New York: Cambridge University Press), pp. 216–240.

Richards, J. A., 1996, Classifier performance and map accuracy. *Remote Sensing of Environment*, **57**, 161–166.

Rignot, E., Williams, C., Way, J.-B., and Viereck, L., 1994, Mapping of forest types in Alaskan boreal forests using SAR imagery. *IEEE Transactions on Geoscience and Remote Sensing*, **32**, 1051–1059.

Roberts, D. A., Smith, M. O., and Adams, J. B., 1993, Green vegetation, nonphotosynthetic vegetation, and soils in AVIRIS data. *Remote Sensing of Environment*, 255–269.

Smith, M. O., Ustin, S. L., Adams, J. B., and Gillespie, A. R., 1990, Vegetation in deserts I. A regional measure of abundances from multispectral images. *Remote Sensing of Environment*, **29**, 1–26.

Steele, B. M., Winne, J. C., and Redmond, R. L., 1998, Estimation and mapping of misclassification probabilities for thematic land cover maps. *Remote Sensing of Environment*, **66**, 192–202.

Stehman, S. V., 1996, Use of auxiliary data to improve the precision of estimators of thematic map accuracy. *Remote Sensing of Environment*, **58**, 169–176.

Stehman, S. V., and Czaplewski, R. L., 1998, Design and analysis for thematic map accuracy assessment: fundamental principles. *Remote Sensing of Environment*, **64**, 331–344.

Stocks, B. J., Fosberg, M. A., Lynham, T. J., Mearns, L., Wotton, B. M., Yang, Q., Jin, J.-Z., Lawrence, K., Hartley, G. R., Maston, J. A., and McKenney, D. W., 1998, Climate change and forest fire potential in Russian and Canadian boreal forests. *Climatic Change*, **38**, 1–13.

Takhtajan, A., 1986, *Floristic Regions of the World* (Berkeley, CA: University of California Press).

USDA SCS, 1977, Soil survey of Goldstream–Nenana area, Alaska. USDA Soil Conservation Service, Palmer, AK.

Ustin, S. L., Roberts, D. A., and Hart, Q. J., 1999, Seasonal vegetation patterns in a California coastal savanna derived from Advanced Visible/Infrared Imaging Spectrometer (AVIRIS) data. In *Remote Sensing Change Detection: Environmental Monitoring Applications and Methods*, edited by C. D. Elvidge and R. Lunetta (Ann Arbor, MI: Ann Arbor Press), pp. 163–180+color plate.

Ustin, S. L., Szeto, L.-H., Xiao, Q.-F., Hart, Q. J., and Kasischke, E. S., 1994, Vegetation mapping of forested ecosystems in Central Alaska. *Proceedings of the International Geoscience and Remote Sensing Symposium IGARSS '94, California Institute of Technology, Pasadena, 8–12 August 1994*.

Van Cleve, K., Dyrness, C. T., Marion, G. M., and Erickson, R., 1993, Control of soil development on the tanana river floodplain, interior Alaska. *Canadian Journal of Forest Research*, **23**, 941–955.

Van Cleve, K., and Viereck, L. A., 1981, Forest succession in relation to nutrient cycling in the boreal forest of Alaska. In *Forest Succession: Concepts and Applications*, edited by D. C. West, H. H. Shugart and D. B. Botkin (New York: Springer-Verlag), pp. 185–211.

Viereck, L. A., 1983, The effects of fire in black spruce ecosystems of Alaska and northern Canada. In *The Role of Fire in Northern Circumpolar Ecosystems*, edited by R. W. Wein and D. A. MacLean (New York: Wiley), pp. 201–220.

Viereck, L. A., Dyrness, C. T., and Foote, M. J., 1993b, An overview of the vegetation and soils of the floodplain ecosystems of the Tanana River, interior Alaska. *Canadian Journal of Forest Research*, **23**, 889–898.

Viereck, L. A., Van Cleve, K., Adams, P. C., and Schlentner, R. E., 1993a, Climate of the Tanana River floodplain near Fairbanks, Alaska. *Canadian Journal of Forest Research*, **2**, 899–913.

Way, J. B., McDonald, K., Paylor, E., Karas, G., Chernobieff, S., and Biery, N., 1992, *Collected Data of the Bonanza Creek Experimental Forest, Alaska*, vol. I and II, *AirSAR and in situ Measurements March 1988, SEASAT SAR July–October 1978* (Pasadena, CA: Radar Science Group, NASA Jet Propulsion Laboratory).

Weber, M. G., and Flannigan, M. D., 1997, Canadian boreal forest ecosystem structure and function in a changing climate: impact on fire regimes. *Environ. Rev.*, **5**, 145–166.

Weber, M. G., and Stocks, B. J., 1998, Forest fires and sustainability in the boreal forests of Canada. *Ambio*, **27**, 545–550.